

Quantum random walks without walking

K. Manouchehri¹ and J.B. Wang^{1,*}

¹*School of Physics, The University of Western Australia*

(Dated: February 17, 2019)

Abstract

Quantum random walks have received much interest due to their non-intuitive dynamics, which may hold the key to a new generation of quantum algorithms. What remains a major challenge is a physical realization that is experimentally viable and not limited to special connectivity criteria. We present a scheme for walking on arbitrarily complex graphs, which can be realized using a variety of quantum systems such as a BEC trapped inside an optical lattice. This scheme is particularly elegant since the walker is not required to physically step between the nodes; only flipping coins is sufficient.

Random walks have been employed in virtually every science related discipline to model everyday phenomena such as the DNA synapsis [1], animals' foraging strategies [2], diffusion and mobility in materials [3] and exchange rate forecast [4]. They have also found algorithmic applications, for example, in solving differential equations [5], quantum monte carlo for solving the many body Schrödinger equation [6], optimization [7], clustering and classification [8], fractal theory [9] or even estimating the relative sizes of Google, MSN and Yahoo search engines [10]. Whilst the so called *classical* random walks have been successfully utilized in such a diverse range of applications, *quantum* random walks are expected to provide us with a new paradigm for solving many practical problems more efficiently [11, 12]. In fact quantum walks have already inspired efficient algorithms with applications in connectivity and graph theory [13, 14], as well as quantum search and element distinctness [15, 16], due to their non-intuitive and markedly different properties including faster *mixing* and *hitting* times.

The question we address in this paper is how to physically implement a quantum random walk in the laboratory. Over the last few years there have been several proposals for such a physical implementation using Nuclear Magnetic Resonance [17], cavity QED [18], ion traps [19], classical and quantum optics [12, 20], optical lattice and microtraps [21, 22] as well as quantum dots [23, 24]. None of the existing proposals however consider quantum random walks on general graphs, with the majority describing only a one-dimensional implementation. This is while from an application point of view most useful algorithms would involve traversing graphs with arbitrarily complex structures.

In this paper, we present a novel scheme which considerably simplifies the evolution of the quantum walk on a general undirected graph. We then describe a systematic procedure capable of performing this quantum walk on a variety of existing as well as prospective quantum computing platforms. Finally we present an example of one such implementation, using a Bose-Einstein condensate (BEC) of ^{87}Rb atoms trapped inside a 2D optical lattice [25].

First we consider a complete graph with all possible connections between the \mathcal{N} nodes including self loops (Fig. 1a). Here the walker requires an \mathcal{N} -sided coin for moving from one node to \mathcal{N} other nodes. The complete state of the walker is therefore described by $|\psi\rangle = \sum_{j=1}^{\mathcal{N}} \sum_{k=1}^{\mathcal{N}} \mathcal{A}_{j,k} |j, k\rangle$, where $\mathcal{A}_{j,k}$ are complex amplitudes, $|j\rangle$ and $|k\rangle$ represent node and coin states respectively. A quantum coin flip corresponds to a unitary rotation of the

coin states at every node j using an $\mathcal{N} \times \mathcal{N}$ matrix \hat{c}_j also known as the coin operator. The coin operation is followed by the walker stepping from node j simultaneously to all other nodes on the graph using a conditional translation operator \hat{T} such that $\hat{T}|j, k\rangle \rightarrow |j', k'\rangle$, where j and j' label the two nodes at the end of an edge $e_{jj'}$ [26]. The quantum walk evolves via repeated applications of the coin followed by the translation operator. More explicitly, we have $|\psi_n\rangle = \hat{T}_n \hat{C}_n \dots \hat{T}_2 \hat{C}_2 \hat{T}_1 \hat{C}_1 |\psi_0\rangle$, where $|\psi_0\rangle$ is the initial state of the walker, $|\psi_n\rangle$ is its state after n steps, \hat{C}_i and \hat{T}_i are the coin and translation operators at the i th step, and \hat{C} incorporates the individual coin operators $\hat{c}_1 \dots \hat{c}_{\mathcal{N}}$ which simultaneously act on all the nodes. The operators \hat{c} can in principle invoke different rotations at each node j , but are often uniformly set to be the Hadamard matrix.

In traversing the edge $e_{jj'}$, we define $\hat{\mathcal{T}}|j, k\rangle \rightarrow |k, j\rangle$ (Fig. 1b). Without undue loss of generality, this choice of translation operator has the unique advantage of being independent of graph connectivity, and thus enabling a quantum walk to be systematically implemented on any arbitrary graph. Upon visualizing the Hilbert space of the walk as an $\mathcal{N} \times \mathcal{N}$ square array \mathcal{H} with entries h_{jk} representing the states $|j, k\rangle$, the application of the translation operator $\hat{\mathcal{T}}$ to the state space of the walk simply becomes equivalent to a transposition of the array elements. Let us now consider the first few steps in the evolution of a quantum walk. Applying \hat{C}_1 to the state space of the walk involves performing \mathcal{N} simultaneous unitary transformations \hat{c}_j , each on the coin states of the node corresponding to the j th row. This leads to a natural grouping of the states along the rows of \mathcal{H} and we employ the relabeled operator \hat{C}_1^H to highlight that it operates on *horizontally* grouped states (Fig. 1c). What is particularly convenient now is that instead of transposing \mathcal{H} due to the action of $\hat{\mathcal{T}}_1$ we can simply transpose the application of the next coin operator \hat{C}_2 . By transposing \hat{C}_2 we mean regrouping the states, this time along the columns of \mathcal{H} , and performing \mathcal{N} simultaneous unitary transformations \hat{c}_j , each on the states of the j th column. As before we employ the relabeled operator \hat{C}_2^V to highlight that it operates on *vertically* grouped states.

In the above formulation, the effect of the translation operator $\hat{\mathcal{T}}$ is implicit in the regrouping of states and does not appear in the expression governing the evolution of the walk, which can now be written as $|\psi_n\rangle = \hat{C}_n^V \hat{C}_{n-1}^H \dots \hat{C}_2^V \hat{C}_1^H |\psi_0\rangle$, reducing the number of required operations to half. It is in this sense that we have qualified this process as a “quantum random walk *without walking*”; the walker is not required to physically step between the nodes, only flipping the coin is sufficient. As we will see, removing the quantum walk’s

dependence on the translation operator \hat{T} greatly facilitates its physical implementation.

We now construct our intended graph \mathcal{G} by simply removing all the unwanted edges (dotted line in Fig. 1a) from its complete counterpart \mathcal{G}_{\max} . In turn this has the effect of removing some of the states from the Hilbert space \mathcal{H} (dotted circle in Fig. 1c). Removing the edge $e_{jj'}$ for example, corresponds to removing two states $|j, j'\rangle$ and $|j', j\rangle$. In our approach however, instead of removing these unwanted states from \mathcal{H} , we simply isolate them from interaction with other states by appropriately designing the coin operators $\hat{c}_1 \dots \hat{c}_{\mathcal{N}}$. Taking \hat{C}^H as an example, matrix \hat{c}_j^H performs a unitary transformation on the j th row of \mathcal{H} . Hence to isolate the state $|j, k\rangle$ we obtain a modified coin matrix whose column elements $c_{1k} \dots c_{\mathcal{N}k}$ and row elements $c_{k1} \dots c_{k\mathcal{N}}$ are all set to zero except for c_{kk} which is 1. Using this modified coin matrix guarantees that if initially the walker has no amplitude in state $|j, k\rangle$, this state will remain unpopulated throughout the evolution of the walk.

It is clear from the preceding discussion that a physical implementation of this walk requires two basic properties commonly found in a variety of systems proposed for traditional quantum computing: (a) \mathcal{N}^2 basis states arranged in a square array formation and (b) implementing the operators \hat{c}_j^H ($\hat{c}_{j'}^V$), which at once perform an \mathcal{N} -state unitary rotation on all the amplitudes in row j (column j') of the 2D state space. Such a mechanism can indeed be efficiently constructed if the system is capable of performing pairwise unitary operations on *non-neighboring* states similar to those demonstrated in [27, 28, 29, 30] and discussed in [31, 32] and references therein. The key to our implementation is a CS decomposition [33] which effectively takes the single unitary operator \hat{c}_j^H ($\hat{c}_{j'}^V$) and replaces it with a series of pairwise operators which we know how to implement. One requirement of this implementation is that $\mathcal{N} = 2^N$ for some integer N , which can introduce some redundancy in the Hilbert space of the quantum walk, but only adds a linear overhead. With the wave function along row j given by $|\psi_j^H\rangle = \sum_{k=1}^{\mathcal{N}} \alpha_k |j, k\rangle \otimes |0\rangle$, we represent the operator \hat{c}_j^H as an $\mathcal{N} \times \mathcal{N}$ unitary matrix acting on a vector $\mathbf{A}_j^H = (\alpha_1 \dots \alpha_{\mathcal{N}})$ of amplitudes in row j . Performing $N - 1$ recursive CS decompositions on \hat{c}_j^H we obtain

$$\hat{c}_j^H = \prod_{i=1}^{N-1} \mathcal{U}_i(d_i), \text{ where } \mathcal{U}_i(d_i) = \begin{pmatrix} u_{i,1} & & \\ & u_{i,2} & \\ & & \ddots \end{pmatrix} \quad (1)$$

and $u_{i,k}$ represent $d_i \times d_i$ square blocks along the \mathcal{U}_i diagonal with $k = 1, 2 \dots \mathcal{N}/d_i$. Block dimensions can vary for each \mathcal{U}_i with values restricted to $d_i = 2, 4, 8 \dots \mathcal{N}/2$. For $d_i = 2$, blocks $u_{i,k}$ represent general 2×2 unitary matrices, but for $d_i > 2$ they assume the special

form

$$u_{i,k} = \left(\begin{array}{c|c} \ddots & \ddots \\ \hline & c_r \\ \hline & -s_r \\ \hline \end{array} \right)_{i,k}, \quad (2)$$

where each quadrant is diagonal with respective entries c_r and s_r corresponding to $\cos(\phi_r)$ and $\sin(\phi_r)$ for some angle ϕ_r and $r = 1, 2 \dots d/2$. The action of each matrix $\mathcal{U}_i(d_i)$ on the vector \mathbf{A}_j^H can now be directly implemented using pairwise interactions. Upon a closer examination of $u_{i,k}$ in Eq. 2 we find that each $c_r s_r$ square block (dotted) performs a pairwise unitary transformation $\bar{u}_{i,k,r}$ on the amplitudes $\alpha_{(k-1)d+r}$ and $\alpha_{(k-1)d+r+d/2}$, which are non-neighboring for $d > 2$. Hence the rotation $\mathcal{U}_i(d_i)$ can be applied at once by simultaneously activating pairwise interactions between all states in the range $|j, kd - d + 1\rangle \dots |j, kd - d/2\rangle$ for all $k = 1, 2 \dots \mathcal{N}/d_i$ and their corresponding counterparts $|j, kd - d/2 + 1\rangle \dots |j, kd\rangle$. Note that conveniently, all interacting pairs of states have the same interval $d/2$ which greatly facilitates the design of a physical implementation.

In the following we describe one such physical implementation using a BEC trapped in a 2D optical lattice [34], where states $|j, k\rangle$ of the walk are encoded using the individual trapping sites and the BEC wave function acts as the quantum walker with some initial distribution throughout the lattice sites. A series of specially tailored control laser operations are introduced to address, manipulate and interact the BEC wave packets in individual sites, in a way that corresponds exactly to the action of the operators \hat{c}_j^H (\hat{c}_j^V) along the lattice rows (columns). Although the control laser wavelength and the lattice period λ_{lattice} are comparable in size, problems associated with unwanted interactions of the control laser with neighboring sites are circumvented by choosing every 2nd, 3rd or ℓ th lattice site to represent the walk states. From an application point of view one would commonly start with the BEC entirely localized in one site or uniformly loaded into every ℓ th site using pattern loading [35]. The system is then driven into a Mott insulator phase [36] thereby suppressing the tunneling between neighboring lattice sites. The design of all subsequent control operations ensures that the initially empty intermediate sites would, in principle, remain unpopulated throughout the walk. In practice however the spatial separation ℓ also acts as a buffer zone to contain any spilling of the BEC out of its confinement lattice-site due to unavoidable experimental imperfections.

To manipulate the trapped BEC wave packet at a given lattice site we propose performing arbitrary unitary transformations on the internal states $|0\rangle \equiv |F = 1, m_F = 1\rangle$ and $|1\rangle \equiv |F = 2, m_F = 2\rangle$ of the BEC with the aid of a pair of three-photon Stimulated Raman Adiabatic Passage (STIRAP) operations [37]. Each STIRAP requires the use of three control lasers (with wavelengths $\sim \lambda_{\text{lattice}}$) applied in the counter intuitive order to transfer the atomic population in states $|0\rangle$ and $|1\rangle$, to and from an auxiliary state $|a\rangle \equiv |F = 2, m_F = 0\rangle$, via an intermediate upper state $|u\rangle \equiv |F' = 1, m_F = 1\rangle$ that does not get populated during the transfer (Fig. 2). The two-photon Λ STIRAP $|1\rangle \longleftrightarrow |u\rangle \longleftrightarrow |a\rangle$ has already been experimentally demonstrated using circularly polarized laser and a magnetic field to lift the degeneracy in the sub-levels m_F [38]. Our proposal simply extends this implementation through the addition of a third linearly polarized laser to facilitate $|0\rangle \longleftrightarrow |u\rangle$.

For performing a unitary transformation of BEC amplitudes in a pair of lattice sites, we utilize a scheme for the spin(state)-dependent transport of neutral atoms in an optical lattice [27, 28]. By setting the wavelength $\lambda_{\text{lattice}} = 785\text{nm}$, internal states $|0\rangle$ and $|1\rangle$ experience different corresponding dipole potentials $\mathcal{V}_0(x, \theta) = \frac{1}{4}V_+(x, \theta) + \frac{3}{4}V_-(x, \theta)$ and $\mathcal{V}_1(x, \theta) = V_+(x, \theta)$, where $V_{\pm}(x, \theta) = V_{\text{max}} \cos^2(kx \pm \theta/2)$, $k = 2\pi/\lambda_{\text{lattice}}$ is the wave vector of the laser light propagating in the x direction, and θ is the relative polarization angle between the pair of counter-propagating lasers. Hence for an atom in the superposition state $\alpha|0\rangle + \beta|1\rangle$, increasing the polarization angle θ will lead to a split in the spatial wave packet of the atom as it perceives a relative motion between the two potentials, resembling that of a pair of conveyor belts moving in opposite directions, each carrying one of the components α and β . The relative displacement is given by $\Delta x = \theta\lambda_{\text{lattice}}/2\pi$.

Let us take a BEC initially prepared in the internal state $|0\rangle$ and distributed between two lattice sites $|j, k\rangle$ and $|j, k'\rangle$ such that $|\psi_0\rangle = \alpha_k|j, k\rangle \otimes |0\rangle + \alpha_{k'}|j, k'\rangle \otimes |0\rangle$. We can now manipulate the amplitudes α_k and $\alpha_{k'}$ according to any desired unitary transformation in five steps depicted in Fig. 3a. (1) Using the three-photon STIRAP we apply a π -rotation to the BEC at $|j, k\rangle$ which transfers it entirely to the internal state $|1\rangle$ and the new state of the system becomes $|\psi_1\rangle = \alpha_k|j, k\rangle \otimes |1\rangle + \alpha_{k'}|j, k'\rangle \otimes |0\rangle$. (2) Making use of the spin(state)-dependant transport, we increase the polarization angle to $\theta = 2\ell(k - k')\pi$ causing the two wave packets to fully overlap at $|j, k'\rangle$ (selected as the stationary reference frame) and hence $|\psi_2\rangle = |j, k'\rangle \otimes (\alpha_k|1\rangle + \alpha_{k'}|0\rangle)$. (3) Using another three-photon STIRAP we perform an arbitrary unitary rotation \hat{R} , this time at $|j, k'\rangle$, such that $|\psi_3\rangle = |j, k'\rangle \otimes (\tilde{\alpha}_k|1\rangle + \tilde{\alpha}_{k'}|0\rangle)$.

(4) Reversing the change in the polarization angle we transport the new BEC amplitudes $\tilde{\alpha}_k$ and $\tilde{\alpha}_{k'}$ back to their original sites, i.e. $|\psi_4\rangle = \tilde{\alpha}_k|j, k\rangle \otimes |1\rangle + \tilde{\alpha}_{k'}|j, k'\rangle \otimes |0\rangle$. (5) Finally performing another π -rotation on the state $|j, k\rangle$ we transfer the BEC back to the internal state $|0\rangle$ producing the desired outcome $|\psi_5\rangle = \tilde{\alpha}_k|j, k\rangle \otimes |0\rangle + \tilde{\alpha}_{k'}|j, k'\rangle \otimes |0\rangle$. Note that internal states $|0\rangle$ and $|1\rangle$ are only used to facilitate the pair-wise interactions and both BEC wave packets will be in their internal ground state $|0\rangle$ before and after they interact.

This scheme can be readily extended to simultaneously activate all the pair-wise interactions required for performing the unitary rotations in Eq. 1. We emphasize that all the \hat{c}_j^H ($\hat{c}_{j'}^V$) operations along the rows (columns) of the optical lattice are performed concurrently, since the structure of the CS decomposition (Eq. 2) is identical for all coin operators and changing the polarization angle θ triggers the same state dependent transport across the entire optical lattice. The effect of using different coin operators for each node appears in step (3), where the control STIRAP can perform different unitary rotations at various lattice sites. At the conclusion of the walk, standard absorption imaging will reveal the BEC densities throughout the entire lattice. The corresponding quantum walk distribution is then derived by integrating the BEC amplitudes over an area $\ell\lambda_{\text{lattice}} \times \ell\lambda_{\text{lattice}}$ centered around the key lattice sites. This will effectively include in the distribution, any residual amplitudes in the neighboring intermediate sites, which are nonetheless substantially lower than the key lattice sites and would therefore have a minimal effect on the final result.

The proposed quantum walk scheme offers a polynomial speedup over an equivalent quantum circuit implementation, highlighting the expected trade off between resource and time scalability. A quantum circuit can in principle represent the walk's Hilbert space using $m = \log_2(\mathcal{N}^2)$ entangled qubits, which is by far more resource efficient. Then, implementing the a generalized $\mathcal{N}^2 \times \mathcal{N}^2$ unitary operator $\hat{\mathcal{T}}_i \hat{\mathcal{C}}_i$ for each step of the quantum walk amounts to performing a m -qubit gate operation that can be realized with around 4^m CNOT gates [39]. Since the quantum circuit can perform at most $m/2$ simultaneous CNOT operations at any one time, each step of the quantum walk requires at least $(4^m)/(m/2) = 2\mathcal{N}^4/\log_2(\mathcal{N}^2)$ operational stages. This is compared to only $\mathcal{N} - 1$ operational stages needed for implementing Eq. 1.

Spin(state)-dependant BEC systems have also been considered as serious contenders for building a quantum computer [40]. This is despite the acute sensitivity of the BEC internal states $|0\rangle$ and $|1\rangle$ to the external magnetic-field environment, leading to phase decoherence

times that are presently in the order of a few ms [29]. Nonetheless, comparing this with a single-site transport time ($\sim 50\mu s$) [27, 28] and STIRAP pulse durations ($\sim 60\mu s$) [38], and also noting the successful realization of spin(state)-dependant BEC transport for up to 7 sites reported in [27], a “proof of principle” implementation (i.e. the first few steps of the walk on an arbitrary graph with a few nodes) should indeed be possible, utilizing the existing experimental techniques. Since our proposed implementation scheme is in fact not inherently bound to any one physical system, naturally as prospective quantum computing hardware grow in scale and fidelity of operations, so will the complexity of graphs on which the quantum walk can be performed.

* Electronic address: wang@physics.uwa.edu.au

- [1] R. B. Sessionsa, M. Orama, M. D. Szczelkuna, and S. E. Halforda, J. Mol. Bio. **270**, 413 (1997).
- [2] O. Bénichou, M. Coppey, M. Moreau, P.-H. Suet, and R. Voituriez, Phys. Rev. Lett. **94**, 198101 (2005).
- [3] Z. T. Trautt, M. Upmanyu, and A. Karma, Science **314**, 632 (2006).
- [4] L. Kilian and M. P. Taylor, J. Int. Eco. **60**, 85 (2003).
- [5] S. Hoshino and K. Ichida, Numer. Math. **18**, 61 (1971).
- [6] D. Ceperley and B. Alder, Science **231**, 555 (1986).
- [7] B. A. Berg, Nature **361**, 708 (1993).
- [8] J. Schöll and E. Schöll-Paschingerb, Pattern Recognition **36**, 1279 (2003).
- [9] C. Anteneodo and W. A. M. Morgado, Phys. Rev. Lett. **99**, 180602 (2007).
- [10] Z. Bar-Yossef and M. Gurevich, in *WWW '06: proceedings* (ACM Press, 2006), pp. 367–376.
- [11] Y. Aharonov, L. Davidovich, and N. Zagury, Phys. Rev. A **48**, 1687 (1993).
- [12] P. L. Knight, E. Roldán, and J. E. Sipe, Phys. Rev. A **68**, 020301 (2003).
- [13] J. Kempe, Contemp. Phys. **44**, 307 (2003).
- [14] B. L. Douglas and J. Wang, J. Phys. A **41**, 075303 (2008).
- [15] N. Shenvi, J. Kempe, and K. B. Whaley, Phys. Rev. A **67**, 052307 (2003).
- [16] A. Childs and J. Goldstone, Phys. Rev. A **70**, 022314 (2004).
- [17] C. A. Ryan, M. Laforest, J. C. Boileau, and R. Laflamme, Phys. Rev. A **69**, 012310 (2004).

- [18] G. S. Agarwal and P. K. Pathak, Phys. Rev. A **65**, 032310 (2005).
- [19] B. C. Travaglione and G. J. Milburn, Phys. Rev. A **65**, 032310 (2002).
- [20] P. Zhang, X. Ren, X. Zou, B. Liu, Y. Huang, and G. Guo, Phys. Rev. A **57**, 052310 (2007).
- [21] J. Joo, P. L. Knight, and J. K. Pachos, J. Mod. Opt. **54** (2007).
- [22] K. Eckert, J. Mompart, G. Birkel, and M. Lewenstein, Phys. Rev. A **72**, 012327 (2005).
- [23] K. Manouchehri and J. Wang, J. Phys. A **41**, 065304 (2008).
- [24] D. Solenov and L. Fedichkin, Phys. Rev. A **73**, 012313 (2006).
- [25] O. Morsch and M. Oberthaler, Rev. Mod. Phys. **78**, Oliver Morsch (2006).
- [26] V. Kendon and B. C. Sanders, Phys Rev A **71**, 022307 (2005).
- [27] O. Mandel, M. Greiner, A. Widera, T. Rom, T. W. Hänsch, and I. Bloch, Phys. Rev. Lett. **91**, 010407 (2003).
- [28] O. Mandel, M. Greiner, A. Widera, T. Rom, T. W. Hänsch, and I. Bloch, Nature **425**, 937 (2003).
- [29] P. J. Lee, M. Anderlini, B. L. Brown, J. Sebby-Strabley, W. D. Phillips, and J. Porto, Phys. Rev. Lett. **99**, 020402 (2007).
- [30] J. Majer, J. M. Chow, J. M. Gambetta, J. Koch, B. R. Johnson, J. A. Schreier, L. Frunzio, and D. I. Schuster, Nature **449**, 443 (2007).
- [31] T. Calarco, U. Dorner, P. S. Julienne, C. J. Williams, and P. Zoller, Phys. Rev. A **70**, 012306 (2004).
- [32] J. Pedersen, C. Flindt, N. A. Mortensen, and A.-P. Jauho, Phys. Rev. B **77**, 045325 (2008).
- [33] A. Edelman and B. D. Sutton, Found. Comput. Math. (2007).
- [34] D. Jaksch, Contem. Phys. **45**, 367 (2004).
- [35] S. Peil, J. V. Porto, B. L. Tolra, J. M. Obrecht, B. E. King, M. Subbotin, S. L. Rolston, and W. D. Phillips, Phys. Rev. A **67**, 051603 (2003).
- [36] I. B. Spielman, W. D. Phillips, and J. Porto, Phys. Rev. Lett. **98**, 080404 (2007).
- [37] Z. Kis and F. Renzon, Phys. Rev. A **65**, 032318 (2002).
- [38] K. C. Wright, L. S. Leslie, and N. P. Bigelow, Phys. Rev. A **77**, 041601 (2008).
- [39] M. M. Juha J. Vartiainen and M. M. Salomaa, Phys. Rev. Lett. **92**, 177902 (2004).
- [40] C. Monroe, Nature **416**, 238 (2002).

FIGURES

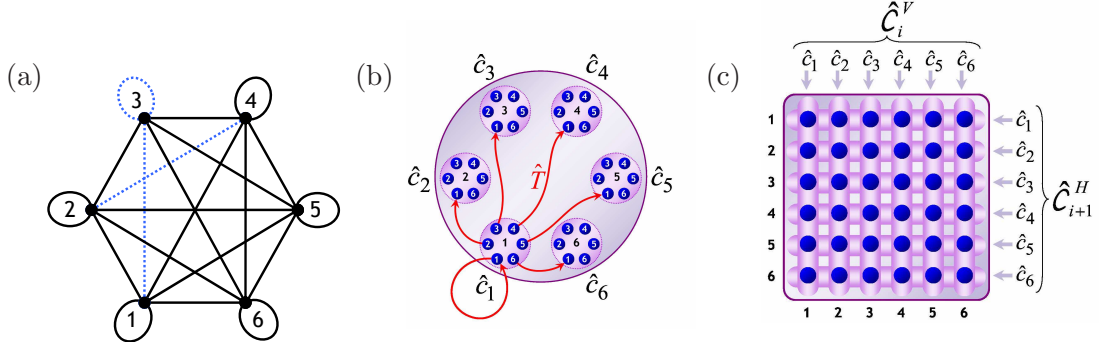


FIG. 1: (a) A complete 6-graph. Any generalized graph can be constructed by removing edges (dotted lines) from the complete graph; (b) Quantum walk Hilbert space and a particular mapping $\hat{T}|j, k\rangle \longrightarrow |k, j\rangle$; (c) \hat{T} is replaced by alternating the direction in which \hat{C} is applied in successive steps of the walk.

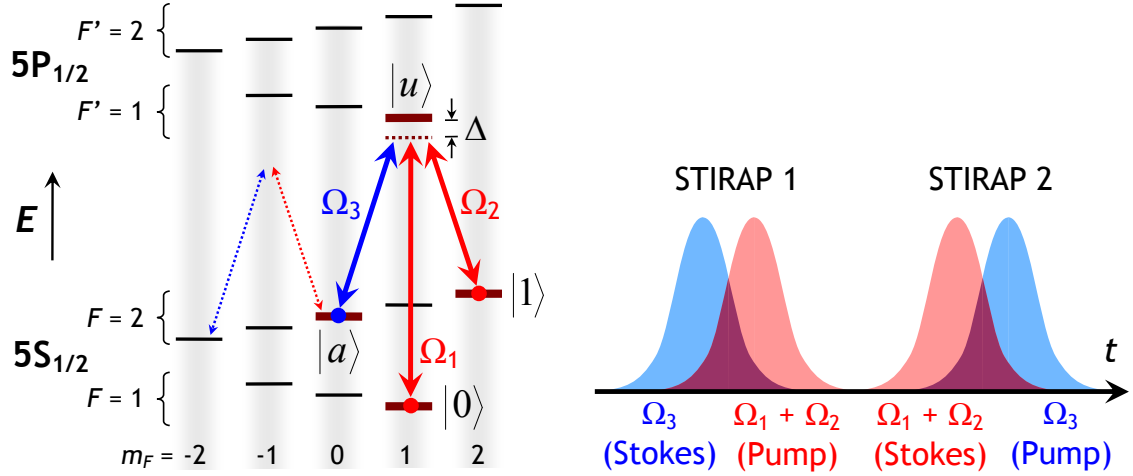


FIG. 2: Schematic diagram of a three-photon STIRAP operation in a ^{87}Rb atom. Internal levels $|0\rangle$, $|1\rangle$, $|a\rangle$ and $|u\rangle$ are coupled by three laser pulses with frequencies Ω_1 , Ω_2 and Ω_3 and polarizations that are linear, left circular σ_- and right circular σ_+ respectively.

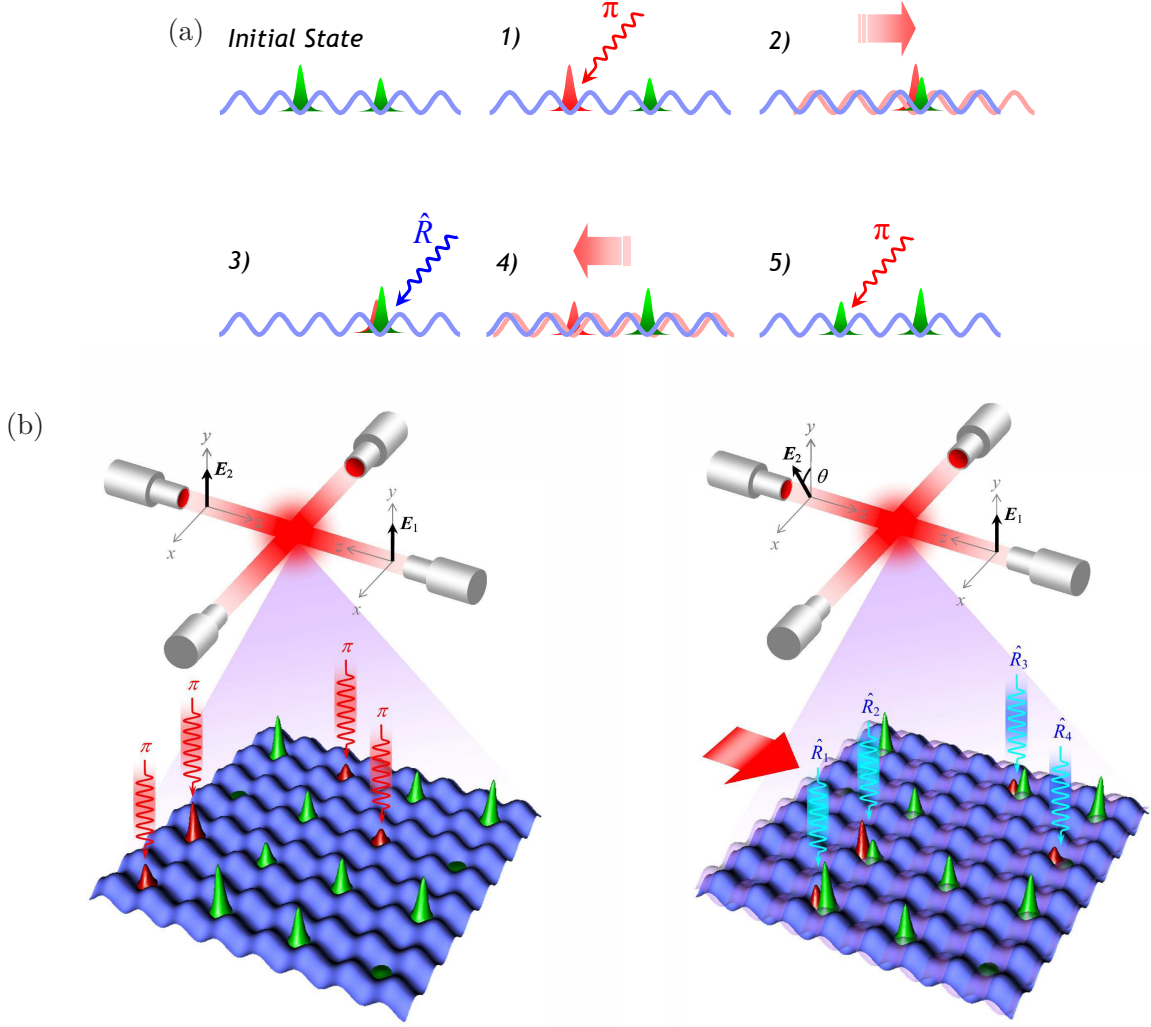


FIG. 3: (a) Steps for applying a unitary transformation to BEC amplitudes trapped in a pair of non-neighboring optical lattice sites; (b) The first three steps on a 2D optical lattice with BEC site separation $\ell = 2$.